

# Direct Numerical Simulation of Multicomponent-Fuel Drop-Laden Temporal Mixing Layers with Phase Change

Patrick C. Le Clercq and Josette Bellan

Jet Propulsion Laboratory, California Institute of Technology  
4800 Oak Grove Drive, MS 125-109  
Pasadena, CA. 91109-8099

## Abstract

A model of a temporal three-dimensional mixing layer laden with a multitude of drops of a fuel containing a large number of species is derived. The drop model is based on continuous thermodynamics, whereby the fuel composition is statistically described through a distribution function, here depending solely on the chemical species molar weight. The drop temperature is initially lower than that of the carrier gas, leading to drop heat up and evaporation. The model describing the evaporation-induced changes in the multicomponent (MC) fuel drop composition and in the gas phase composition, due to evaporation, encompasses only two more conservation equations when compared with the equivalent single-component (SC) fuel formulation. The new physics embedded in the MC formulation is demonstrated by comparing results from MC-fuel drop simulations with those of an SC-fuel typically used to represent the MC-fuel. Further, two mixing layer simulations were conducted with SC-fuel and MC-fuel drops, respectively. Analysis of the results shows that although the global layer characteristics are similar in the SC and MC situations, the layer detailed structures are different. The MC-fuel drop layer exhibits a more complex structure than its SC counterpart. This is attributed to the slower evaporation rate of the MC-fuel drops, which permits an increased interaction of the drops with the flow, resulting in a more developed small scale structure. This slower evaporation also leads to higher drop number density regions in the MC-fuel drop-laden layer. A segregation of gas phase species is detected in the MC-fuel layer based on the relative evaporation time from the drops.

## Introduction

Most power producing combustion devices employ sprays of commercial petroleum fuels that typically contain hundreds of pure species. Despite the preponderance of multicomponent (MC) fuels, the specific behavior of such sprays in turbulent flows is not well understood when compared to that of sprays of single-component (SC) fuels. The goal of the present study is to understand the specific difference between MC-fuel and SC-fuel two-phase turbulent flows by taking as a representative example a drop-laden mixing layer.

To achieve this goal, the present study employs Direct

Numerical Simulations (DNS) to investigate the behavior of a temporal mixing layer whose lower stream is initially laden with a large number of evaporating MC-fuel drops. DNS studies with solid particles in the absence of phase change were previously performed by Boivin et al. [1], and by Mashayek and Jaber [2] in the context of isotropic turbulence; by Mashayek [3], who investigated evaporating drops in isotropic turbulence; by Réveillon and Vervisch [4] who studied clusters and randomly distributed evaporating SC-fuel drops in a three-dimensional (3D) freely decaying turbulence; by Mashayek [5] who explored evaporating drops in homogeneous shear; and by Miller and Bellan [6] [7] who studied 3D mixing layers with evaporating SC-fuel drops. The present DNS methodology generally follows that of [6], while the drop model is developed in the context of continuous thermodynamics ([8], [9], [10], [11], [12]) and is therefore entirely novel in the context of mixing layers.

## Mathematical model

The governing equations are formulated in an Eulerian-Lagrangian frame for the gas and drops, respectively. This representation is consistent with the volumetrically small loading ( $\approx 10^{-3}$ ), although the mass loading can be substantial due to the very high density ratio between the liquid and carrier gas ( $O(10^3)$ ). Moreover, the drops are treated as point sources of mass, momentum and energy. This representation is consistent with the drop size being smaller than the Kolmogorov scale (see discussion in [1]). The carrier gas is assumed calorically perfect. Due to space restrictions, only the highlights of the model are presented, and the reader is referred to a detailed derivation elsewhere [13].

## Continuous thermodynamics for single multicomponent fuel drops

The primary idea of CT modeling is to describe the fuel composition (both liquid or vapor) using a distribution function,  $f$ . Although generally  $f$  depends on many parameters representing the characteristics of the fuels, it has been shown [9], [11] that in certain cases it is possible to reduce this dependency to a single parameter, the species molar weight. This simplification is available for mixtures composed of homologous species [8] [9], and in-

cludes diesel and gasoline fuels [9] [10], which are of major practical interest. The advantage of such a statistical description is that while a wide range of individual species can be accommodated in the mixture, the number of governing equations is minimally augmented with respect to that necessary for a single species because the composition is represented by a small number of parameters determining  $f$ .

In CT,  $f$  is used to define the mole fraction of species  $\alpha$ ,  $X_\alpha$ , whose molar weight lies within the range  $m_\alpha$  to  $m_\alpha + \Delta m_\alpha$  through

$$X_\alpha = f(m_\alpha)\Delta m_\alpha, \quad \int_0^\infty f(m_\alpha) dm_\alpha = 1. \quad (1)$$

Whitson [14] has shown that gamma distributions may be used to characterize the high molar-weight portion of crude oils through

$$f(m) = \frac{(m-\gamma)^{\alpha-1}}{\beta^\alpha \Gamma(\alpha)} \exp\left[-\left(\frac{m-\gamma}{\beta}\right)\right], \quad (2)$$

where  $\Gamma(\alpha) = (\alpha-1)!$ . The origin of  $f$  is specified by  $\gamma$ , and its shape is determined by two parameters,  $\alpha$  and  $\beta$ . These parameters are related to the mean,  $\theta$ , the variance,  $\sigma^2$ , and the second moment,  $\psi$ , of  $f$  by

$$\theta = \alpha\beta + \gamma, \quad \sigma^2 = \alpha\beta^2, \quad \psi = \theta^2 + \sigma^2. \quad (3)$$

#### Gas phase conservation equations

If the overall vapor mole fraction is  $X_v$ , the carrier gas mole fraction is  $X_{ga} = 1 - X_v$ , and the vapor phase mole fraction of species  $\alpha$  is defined through

$$X_\alpha = X_v [f_v(m_\alpha)] \Delta m_\alpha. \quad (4)$$

Multiplying eq. 1 by  $m_\alpha$  and by  $m_\alpha^2$  and integrating it for infinitesimally small  $\Delta m_\alpha$ , yields the mean molar weight of the vapor,  $\theta_v = \int_0^\infty f_v(m_\alpha) m_\alpha dm_\alpha$  and the second moment  $\psi_v = \int_0^\infty f_v(m_\alpha) m_\alpha^2 dm_\alpha$ , respectively.

In discrete form, the mean molar weight,  $m$ , is defined as

$$m = m_{ga} X_{ga} + \sum_{\alpha=1}^N m_\alpha X_\alpha \quad \alpha \in \text{fuel}, \quad (5)$$

where  $N$  is the total number of species in the fuel, and the equivalent expression in continuous form is

$$m = m_{ga}(1 - X_v) + \theta_v X_v. \quad (6)$$

The gas phase is considered to be a mixture of perfect gases and thus

$$p = \frac{\rho R_u T}{m} = c R_u T \quad (7)$$

where  $\rho = mc$  is the mass density of the gas mixture,  $p$  is the thermodynamic pressure,  $R_u$  is the universal gas constant,  $T$  is the temperature and  $c$  is the molar density.

The gas phase conservation equations are derived as in [10] from the unsteady discrete form of the molar fraction conservation and enthalpy equations

$$\frac{\partial(cX_\alpha)}{\partial t} + \nabla \cdot (cX_\alpha \mathbf{u}^*) = \nabla \cdot (cD_\alpha \nabla X_\alpha), \quad (8)$$

$$C_{pv} \frac{\partial(cT)}{\partial t} + C_{pv} \nabla \cdot (cT \mathbf{u}^*) = \nabla \cdot (\lambda_v \nabla T) - \nabla \cdot \left( \sum_{\alpha=1}^N \mathbf{J}_{D_\alpha} h_{v\alpha} \right). \quad (9)$$

This derivation involves taking the mean and first two moments of eq. 8 and the mean of eq. 9 with respect to  $f$  to yield conservation equations for  $cX_\alpha$ ,  $cX_\alpha m_\alpha$ ,  $cX_\alpha m_\alpha^2$  and enthalpy in CT form. A detailed derivation of the equations is available elsewhere [10],[13].

#### Liquid phase conservation equations

The conservation equations for the liquid phase are here obtained under the assumption of a well-mixed liquid, meaning that internal circulation is very effective and renders the properties of the drop uniform in a time much shorter than the drop lifetime. This assumption is consistent with a relatively slow evaporation, which is the situation pertinent to the present mixing layer simulations. Departures from this well-mixed state are expected to become increasingly important with wider separation of the saturation vapor pressure curves for different species, however, for a continuous mixture these departures may be considerably reduced. Following the CT derivation and approximations of [10], the conservation equations for a spherically symmetric drop are

$$\frac{d\theta_l}{dt} = \frac{6}{c_l d} [J_r(\theta_l - \theta_v X_v) + c\tilde{D} \nabla(X_v \theta_v)]_s, \quad (10)$$

$$\frac{d\psi_l}{dt} = \frac{6}{c_l d} [J_r(\psi_l - \psi_v X_v) + c\hat{D} \nabla(X_v \psi_v)]_s, \quad (11)$$

$$\frac{dT_d}{dt} = \frac{6}{C_l c_l d} [q_s - L_v], \quad (12)$$

where  $J_{rs} = (\underline{dN}_d/dt)A$  is the radial molar flux at the drop surface,  $\tilde{D}$  and  $\hat{D}$  are averaged diffusion coefficients [13],  $N_d = M_d/\theta_l$  is the number of moles in the drop,  $M_d$  is the drop mass (subscripts  $d$  and  $l$  refer to the drop and liquid),  $A = \pi d^2/4$  is the drop area,  $d$  is the drop diameter,  $c_l$  is the liquid molar density,  $C_l$  is the liquid heat capacity at constant pressure,  $q_s$  is the heat flux at the drop surface and  $L_v$  is the liquid latent heat. The rapid mixing assumption implies that  $T_d = T_s$ .

#### Boundary conditions

The boundary conditions are applied both in the far field of the drop, and at the drop surface where special care must be devoted to obtain a consistent phase coupling. The far field values of the dependent variables are specified through the given gas composition and temperature; all these values are denoted by the subscript  $e$ . The result of

these manipulations is to obtain the CT form of the boundary conditions which yields relationships between  $X_{vs}$  and the distribution parameters in the liquid, and between the distribution parameters in the liquid and vapor

$$X_{vs} = \frac{p_{atm} \exp[\Delta s_{fg}/(R_u T_s) (T_s - A_b - \gamma B_b)]}{p_e (1 + \Delta s_{fg}/(R_u T_s) B_b \beta_l)^{\alpha_l}}, \quad (13)$$

$$\theta_{vs} - \gamma = \frac{\theta_l - \gamma}{1 + \frac{(\Delta s_{fg}/R_u) (1 - A_b/T_s) (B_b/(T_s - A_b)) \sigma_l^2}{\theta_l - \gamma}}, \quad (14)$$

$$\sigma_{vs}^2 = \sigma_l^2 \left[ \frac{\theta_{sv} - \gamma}{\theta_l - \gamma} \right]^2, \quad (15)$$

having assumed that  $\gamma_l = \gamma_{vs} = \gamma$ . In eqs. 13 - 15 the entropy of vaporization  $\Delta s_{fg}$ , can be expressed using Trouton's empirical law  $\Delta s_{fg} = L_v/T_b \simeq 87.9 \text{ J K}^{-1} \text{ mol}^{-1}$  and  $T_b(m_\alpha) = A_b + B_b m_\alpha$ , where the coefficients  $A_b$  and  $B_b$  are constants and listed in [10].

### Mixing layer conservation equations

#### Gas phase conservation equations

The gas phase formulation of [6] is here modified in three ways. First, two transport equations, for  $\theta_v$  and  $\psi_v$ , are added to represent the entire molar weight range of evaporated fuel species;  $\psi_v$  is used as a primitive variable instead of the  $\sigma^2$  (as in the drop model) because the resulting equation is simpler. Second, as in Okong'o and Bellan [15], the influence of the diffusion velocities in the heat flux vector are included. Finally, since all available thermophysical property correlations [16], [10] utilize  $m_\alpha$ , for consistency reasons two of the primitive variables are now  $c$  and  $X_\alpha$  instead of  $\rho$  and the mass fractions,  $Y_\alpha = X_\alpha m_\alpha/m$ . The equations are:

$$\frac{\partial c}{\partial t} + \frac{\partial}{\partial x_j} [c u_j] = -\frac{c}{m} \frac{Dm}{Dt} + \frac{S_{I-\text{mass}}}{m}, \quad (16)$$

$$\frac{\partial (\rho u_i)}{\partial t} + \frac{\partial}{\partial x_j} [\rho u_i u_j + p \delta_{ij} - \tau_{ij}] = S_{II,j}, \quad (17)$$

$$\begin{aligned} \frac{\partial (\rho e_t)}{\partial t} + \frac{\partial}{\partial x_j} \left[ (\rho e_t + p) u_j - \lambda \frac{\partial T}{\partial x_j} - u_i \tau_{ij} \right] \\ + \frac{\partial}{\partial x_j} \left[ \sum_{\beta=[ga,[1,N]]} J_{Dj\beta} h_\beta \right] = S_{III}, \end{aligned} \quad (18)$$

$$\frac{\partial (c X_v)}{\partial t} + \frac{\partial}{\partial x_j} \left( c X_v u_j - c \bar{D} \frac{\partial X_v}{\partial x_j} \right) = S_{I-\text{mole}}, \quad (19)$$

$$\frac{\partial (c X_v \theta_v)}{\partial t} + \frac{\partial}{\partial x_j} \left[ c X_v \theta_v u_j - c \tilde{D} \frac{\partial (X_v \theta_v)}{\partial x_j} \right] = S_{I-\text{mass}}, \quad (20)$$

$$\frac{\partial (c X_v \psi_v)}{\partial t} + \frac{\partial}{\partial x_j} \left[ c X_v \psi_v u_j - c \hat{D} \frac{\partial (X_v \psi_v)}{\partial x_j} \right] = S_\psi, \quad (21)$$

where  $j$  denotes the Cartesian coordinate,  $\mathbf{u}$  is the velocity of the mean mass and  $S_{I-\text{mass}} = \sum_{\alpha=1}^N S_{I\alpha-\text{mass}}$  is the mass source due to evaporation where  $S_{I\alpha-\text{mass}}$  is the evaporated mass of  $\alpha$ -species from the drop,  $\tau_{ij} = \mu [2S_{ij} - (2/3)S_{kk}\delta_{ij}]$  is the stress tensor with  $S_{ij} = (1/2)(\partial u_i/\partial x_j + \partial u_j/\partial x_i)$  where  $\delta_{ij}$  is the Kronecker delta function,  $S_{II}$  is the momentum source due to the drop-gas interaction, and  $S_\psi$  is the source of  $c X_v \psi_v$  in the gas phase due to drop evaporation. The perfect gas equation of state,  $p = c R_u T$ , is used to close the system of gas phase equations.

#### Individual drop governing equations

Coupled to the gas phase conservation equations, the drop equations for the position,  $\chi$ , the velocity,  $\mathbf{v}$ ,  $T_d$ ,  $\theta_l$  and  $\psi_l$  are

$$\begin{aligned} \frac{d\chi_i}{dt} &= v_i, \\ \frac{dv_i}{dt} &= \frac{F_i}{M_d}, \\ \frac{dT_d}{dt} &= \frac{Q + (dN/dt)L_v}{N C_l}, \\ \frac{d\theta_l}{dt} &= \frac{6J_{rs}}{c_l d} \left[ \theta_l + \frac{\theta_v X_v - \theta_{vs} X_{vs} (1+B)}{B} \right], \\ \frac{d\psi_l}{dt} &= \frac{6J_{rs}}{c_l d} \left[ \psi_l + \frac{\psi_v X_v - \psi_{vs} X_{vs} (1+B)}{B} \right], \end{aligned} \quad (22)$$

where according to [11]

$$J_{rs} = \frac{c\bar{D}}{d/2} \ln(1+B) \quad \text{with } B = \frac{X_{vs} - X_v}{1 - X_{vs}} \quad (23)$$

where  $B$  is the CT equivalent of the Spalding transfer number [17]. The force term,  $F_i$ , the heat transfer term,  $Q$ , and the enthalpy associated with the evaporation  $L_v(dN/dt)$  account for the coupling between the gas and the drops. The values of the gas phase variables ( $u_i, T, X_v, \theta_v, \psi_v$ ) at the drop location serve now as the far field boundary conditions for the single drop equations presented above. Using the validated models for  $F_i, Q$  and  $dN/dt$  described in Miller et al. [18], one obtains

$$\begin{aligned} F_j &= \left( \frac{M_d}{\tau_d} \right) f_1 (u_j - v_j) \\ Q &= \left( \frac{M_d}{\tau_d} \right) \frac{Nu C_{pg}}{3 Pr m} f_2 (T_g - T_d) \\ \frac{dN}{dt} &= J_{rs} \frac{\pi d^2}{4} = - \left( \frac{M_d}{\tau_d} \right) \frac{Sh}{3 Sc m} \ln(1+B) \end{aligned} \quad (24)$$

where  $\tau_d = \rho_l d^2/(18\mu)$  is the particle time constant for Stokes flow, and  $\mu$  is the viscosity of the carrier gas;  $Pr = \mu C_{pg}/(\lambda m)$  and  $Sc = \mu/(\rho \bar{D})$  are the Prandtl and the Schmidt numbers respectively. The Nusselt,  $Nu$ , and the Sherwood,  $Sh$ , numbers are semi-empirically modified to account for convective effects in the heat and the mass transfer using the Ranz-Marshall correlations (see the detailed relationships in [6]).  $f_1$  is an empirical correction

to Stokes drag accounting for both finite droplet Reynolds numbers ( $Re_d = \rho \|\mathbf{u} - \mathbf{v}\| d/\mu$ ) and a Reynolds number based on the blowing velocity ( $Re_b = \rho U_b d/\mu$ , with  $U_b = J_{rs}/c$ ) due to evaporation; the exact relationship for  $f_1$  is listed in [6].  $f_2$  is an analytical correction to heat transfer due to evaporation:  $f_2 = \kappa/(\exp(\kappa) - 1)$  where  $\kappa = -1.5 \text{Pr} \tau_d(dN/dt)/N$ . Finally,  $\mu$  is computed from the specified initial (subscript 0) Reynolds number,  $Re_0$ ,  $\mu = \rho \Delta U_0 \delta_{\omega,0}/Re_0$ , where  $\Delta U_0 = 2U_0$  is the initial difference in the freestream velocities calculated from the specified initial Mach number,  $M_{c,0}$  (see details in [6]), and  $\delta_{\omega,0}$  is the initial vorticity thickness. The specification of  $\text{Pr}$ ,  $Sc$  and  $Re_0$  leads to a family of gas phase solutions that is independent of the actual ratios  $\mu/\lambda$  and  $\mu/\bar{D}$ ; this is the principle of flow similarity. However, the drop characteristic time  $\tau_d$  depends explicitly on  $\mu$ , meaning that the  $\mu$  magnitude will influence the drop interaction with the flow. The choice of the  $\tau_d(\mu)$  value is intended to render the drop and flow characteristic times of same order of magnitude so as to enable the investigation of their interaction.

### Source terms

The source terms in eqs. 16 - 21 express the phase coupling of mass, momentum, energy and composition. Using conservation principles, one obtains

$$\begin{aligned}
S_{I\text{-mass}} &= - \sum_{q=1}^{N_d} \frac{w_q}{\Delta x^3} \left[ \frac{d(N\theta_l)}{dt} \right]_q, \\
S_{I\text{-mole}} &= - \sum_{q=1}^{N_d} \frac{w_q}{\Delta x^3} \left[ \frac{dN}{dt} \right]_q, \\
S_{II,j} &= - \sum_{q=1}^{N_d} \frac{w_q}{\Delta x^3} \left[ F_j + \frac{d(N\theta_l)}{dt} v_j \right]_q, \\
S_{III} &= - \sum_{q=1}^{N_d} \frac{w_q}{\Delta x^3} \left[ \frac{v_j F_j}{\theta_l} + Q + \frac{dN}{dt} \left( \frac{v_j v_j}{2} + h_{v,s} \right) \right]_q, \\
S_{\psi} &= - \sum_{q=1}^{N_d} \frac{w_q}{\Delta x^3} \left[ \frac{d(N\psi_l)}{dt} \right]_q,
\end{aligned}$$

where the summations are over all drops residing within a local numerical discretization volume,  $\Delta x^3$ , and a geometrical weighting factor  $w_q$  is used to distribute the individual drop contributions to the nearest eight grid points in proportion to their distance from the drop location.  $h_{v,s} = C_l T_s + L_v$  is the enthalpy of the evaporated vapor.

### Single MC-fuel drop results

Before undertaking DNS of the mixing layer with MC-fuel drops it is important to build confidence in the ability of the CT method to portray the physics of fuel mixtures. To establish the difference in baseline behavior between different MC fuels, several MC-fuel drop calculations were

conducted. The parameters characterizing  $f$  for all the fuels used in the computations are listed in Table 1. The values of  $\theta_{l,0}$  and  $\sigma_{l,0}$  are prescribed, whereas  $\gamma_{l,0}$  is calculated from the condition that  $T_{d,0} < T_{b,0}$  and therefore  $\gamma_{l,0} = (T_{d,0} - A_b)/B_b$ , meaning that it corresponds to the species having the lowest boiling point.

The results plotted in Fig. 1 are all for  $T_{ge} = 1000$  K,  $T_{d,0} = 300$  K,  $Re_{d,0} = 0$  and  $d_0 = 10^{-4}m$ . For diesel fuel, which is the least volatile fuel, an enlarged heating period is necessary before initiating vaporization, and thus its lifetime (Fig. 1a) is largest. The heating period of gasoline is slightly shorter than that of  $n$ -decane because the lighter species in gasoline mixtures are more volatile, however, as the heavier species begin evaporating in gasoline, the drop evaporation rate decreases with respect to  $n$ -decane. Illustrated in Fig. 1b is the time evolution of  $T_d$  for the  $n$ -decane and diesel fuel drops, as well as  $T_b$  for the diesel fuel drop. In both situations,  $T_d$  is bounded by  $T_b$ ; for  $n$ -decane, an asymptotic  $T_d$  behavior is reached, however, no such situation occurs for the diesel drop whose  $T_b$  evolves with the composition. Comparing the initial diesel drop composition with that at half way through the drop lifetime (see Fig. 1c), one discerns the disappearance of the lighter species and the concomitant higher peak at a larger molar weight. To further quantify the diesel drop evolution, the surface vapor mole fraction is displayed in Fig. 1d as a function of  $t$ . Following the initial transient during which  $X_{v,s}$  continuously increases, a stationary state is reached corresponding to a quasi-steady evaporation. Therefore, it is of interest to explore if the different evolution of MC-fuel drops when compared to that of SC-fuel drops may affect the characteristics of drop-laden mixing layers.

### Mixing layer results

To explore the approximations introduced by the SC assumption, two DNS simulations of a drop-laden mixing layer are compared for the same conditions except for the identity of the fuel in the drops. The present simulation using diesel fuel is compared with that of [15] using  $n$ -decane (a common simulant of Diesel fuel).

### Numerical procedure, initial and boundary conditions

Figure 2 shows the computational domain configuration and the definition of the streamwise,  $x_1$ , cross-stream,  $x_2$ , and spanwise,  $x_3$ , coordinates with lengths  $L_1 = 4\lambda_1 = 29.16\delta_{\omega,0}$ ,  $L_2 = 1.1L_1$ , and  $L_3 = 4\lambda_3 = 0.6L_1$ , with  $L_1 = 0.2m$ . The parameters  $\lambda_1$  and  $\lambda_3$  are forcing wavelengths in the  $x_1$  and  $x_3$  directions, and were used to excite the layer in order to induce rollup and pairing as in Moser and Rogers [21], [6] and [7].  $\delta_{\omega,0} = \Delta U_0 / \langle \partial u_1 / \partial x_2 \rangle$  where the brackets  $\langle \rangle$  indicate averaging over homogeneous ( $x_1 - x_3$ ) planes, is the initial vorticity thickness and the initial condition for  $u_1$  is presented in [6]; for this initial condition  $\delta_{\omega,0} = 6.85 \times 10^{-3}m$ . The drops were

distributed randomly throughout the lower stream with uniform number density and a uniform temperature. The initial drop slip velocity with respect to the gas was null, and the initial drop size distribution was polydisperse and specified by the Stokes number,  $St = \tau_d \Delta U_0 / \delta_{\omega,0}$  (both  $\langle St_0 \rangle$  and  $St_{0,rms}$ ). Table 2 summarizes initial conditions, where the SC mixing layer results represent the database originated by Okong'o and Bellan [15].  $Re_0$  was chosen small enough to obtain resolution of all scales. The mass loading,  $ML$ , is defined as the total mass of the liquid relative to the total mass of the gas in the laden stream at  $t = 0$ . Furthermore, in both simulations  $M_{c,0} = 0.4$  and  $Pr = Sc = 0.67$ .

The numerical mesh used in the simulation was uniform in all directions and the resolution was  $256 \times 288 \times 160$  in both simulations. The boundary conditions in the  $x_1$  and  $x_3$  directions were periodic and adiabatic slip-wall conditions in the  $x_2$  direction previously derived by Poinot and Lele [19] and Baum et al. [20], based on the wave decomposition method, were here adapted to the CT model for MC mixtures.

The governing equations were solved numerically using a fourth-order explicit Runge-Kutta temporal integration for all time derivatives and eighth-order central finite differences for all spatial derivatives. A fourth-order Lagrange interpolation procedure was used to obtain gas phase variable values at drop locations. As drops evaporate, their residual mass decreases. Drops whose residual mass was less than 3% were removed from the calculation. The initial conditions for the temporally developing mixing layer configuration were based on those of Moser and Rogers [21] and were detailed in [6].

### Global layer evolution

To compare SC and MC simulations, the global evolution of the layers through the momentum thickness,  $\delta_m$

$$\delta_m = \frac{1}{(\theta_1 - \theta_2)^2} \int_{-L_{2,\min}}^{L_{2,\max}} -(\theta_2 + \langle \rho u_1 \rangle)(\theta_1 + \langle \rho u_1 \rangle) dx_2 \quad (25)$$

was first examined, with  $\theta_1 = \langle \rho u_1 \rangle_{x_2=L_{2,\max}}$  and  $\theta_2 = \langle \rho u_1 \rangle_{x_2=-L_{2,\min}}$ ,  $L_{2,\max} = -L_2/2$  and  $L_{2,\min} = L_2/2$ . Illustrated in Fig. 3 is  $\delta_m / \delta_{\omega,0}$  as a function of  $t^* = t \Delta U_0 / \delta_{\omega,0}$  for both SC-fuel and MC-fuel drop-laden layers. Both layers display rollup and a double pairing, with a plateau after the first pairing indicative of the forcing effect. The second pairing was completed at  $t^* = 87$ , at which time the simulations were stopped. One discerns practically no difference between the SC and MC layer growth, which is apparently unaffected by the liquid composition in the drops.

Owing to the major role of the vorticity,  $\omega \equiv \nabla \times \mathbf{u}$ , in turbulent flows, global aspects of the flow that are associated with  $\omega$  were also examined. In Figs. 4a and 4b the volume averaged non-dimensional positive spanwise vorticity,  $\langle \langle \omega_3^+ \rangle \rangle \delta_{\omega,0} / \Delta U_0$ , and the non-dimensional enstrophy,  $\langle \langle \omega_i \omega_i \rangle \rangle (\delta_{\omega,0} / \Delta U_0)^2$ , evolutions are depicted

as functions of  $t^*$ ; here  $\langle \langle \rangle \rangle$  denotes volume averaging. The positive spanwise vorticity (Fig. 4a) begins increasing after rollup, and following the plateau displayed after the first pairing, continues to increase at a sustained rate. A similar behavior is portrayed in 4b for the enstrophy. Both the positive spanwise vorticity and the enstrophy seem insensitive to the fuel composition. This finding is totally consistent with an examination of the  $\omega$  and  $\omega \cdot \omega$  budgets showing that at  $t^* = 87$  source terms were negligible with respect to the other terms.

### Visualizations after completion of the second pairing

Visualizations of detailed features of the flow were examined to determine if local aspects of the dependent variables show the insensitivity to the fuel composition exhibited by the global quantities. Since in combustion applications the local variables govern the reaction rates, the local comparison of the vorticity, drop number distribution and features associated with the gaseous fuel composition is very pertinent.

Figures 5a and 5b show  $\omega_3$  in the between-the-braid plane for the SC (Fig. 5a) and MC (Fig. 5b) layers at  $t^* = 87$ . Although the major visual features of the flow are similar in the two cases, the details display marked differences. The maximum positive spanwise vorticity is smaller for the MC-fuel drop-laden layer, indicating that a wide spread molar weight liquid fuel composition may reduce the vorticity magnitude in the flow; this conclusion is consistent with the vorticity and vorticity-magnitude budget analyses. Although the general level of vorticity activity is higher in the SC-fuel layer, locally one observes considerably more numerous high vorticity regions for the MC-fuel mixing layer. These more numerous sites of very high vorticity are expected to lead to a more highly-structured flow by inducing the formation of high drop number density regions through flinging the drops away from the high to the low vorticity locations. This interpretation is supported by visualizations of the drop number density in Fig. 6 and is in agreement with the results of Squires and Eaton [22] who found that particles with a density larger than that of the carrier flow concentrate in regions of low vorticity and high strain. The noteworthy feature in Fig. 6 is the small-scale structure formed, with drops profiling the small-scale vortices. The highest drop concentration is not at the periphery of the coherent vortex representing the ultimate structure resulting from the two pairings of the four initial vortices, but rather at the periphery of small-scale vortical structures. Comparing the drop number distribution for the SC and MC simulations (Figs. 6a and 6b), it appears that in the latter situation there is an increased small-scale structure, corresponding to the increased complexity of the vorticity field. This increased small-scale structure is accompanied by a higher maximum drop number density. The smaller drop number density obtained in the SC simulation is attributed to the faster drop evaporation compared to the MC coun-

terpart [13], resulting in some drops becoming completely evaporated and being removed from the calculation. In contrast, none of the MC-fuel drops satisfy the criterion for complete evaporation.

The resulting mass fraction of the evaporated species (not shown) exhibits a considerably smaller amount of vapor for the MC layer, which is attributed to the wide range of species volatility that leads to a decreasing evaporation rate once the most volatile components have been released. In Fig. 7 the distribution of molar weight in the gas phase is exhibited for the MC simulation. The wide range of molar weights is noteworthy, and should be compared to the constant molar weight of *n*-decane, 142 kg/kmole. The lightest components, which egress from the drop early during evaporation, reside in the lower stream. The intermediary molar weight components accumulate mostly in the interior of the layer, as they have been released after the drops were entrained in the layer and have thus participated in the mixing process. In contrast, the heaviest components reside in the regions of high number density, as they evaporate later during the drop lifetime and have not participated in the mixing. Therefore, a segregation of chemical species becomes established according to the time when they were released from the drops. This segregation can obviously not be captured by SC-fuel drop-laden mixing layer simulations.

### Conclusions

A study of a multicomponent drop-laden three-dimensional mixing layer has been conducted by adopting the continuous thermodynamics approach to mathematically describe the fuel composition in a probabilistic manner. Initially, the layer is laden with drops in the lower stream and the drop temperature is lower than that of the carrier gas. Drop heat up leads to evaporation and thus to a change in the gas phase composition. Following previous continuous thermodynamics representations, the distribution of the chemical species in the fuel (whether liquid or gas) is described by a function of the molar weight. A model for the MC-fuel drop-laden mixing layer has been developed by assuming the initial mathematical form of the distribution function and postulating that the same form is retained during the drop lifetime, but with evolving mean and variance as the drops evaporate. Therefore, the physical complexity of the MC situation was mathematically translated to only two additional equations being solved (one for the mean, and one for the variance) for each liquid and gas. Isolated multicomponent-fuel drop calculations were conducted with diesel and gasoline fuels to elucidate their behavior when compared to that of *n*-decane.

The results from two mixing layer simulations were compared, where one simulation was conducted with *n*-decane drops and the other was performed with diesel-fuel drops. Except for the liquid properties (density, composition and thermophysical properties), all initial conditions were the same in both calculations. The mixing layer

simulations consisted of the perturbation-induced double pairing of four initial vortices to yield an ultimate vortex within which small scales proliferate. Although the global properties of the layers (momentum thickness, enstrophy, positive spanwise vorticity and vorticity budgets) were found to be similar, visualizations showed that the details of the layers differ. Because multicomponent-fuel drops evaporate slower due to the higher saturation pressure of the heavier species, their interaction time with the flow is longer. This larger interaction time leads to the development of a more complex small-scale vorticity structure in the flow, and to the creation of regions of higher drop number density than in the single-component fuel simulation. The last feature is the result of single-component fuel drops becoming evaporated, and thus being removed from the computation. In the single-component case, the molar weight of the evaporated fuel is inherently constant. For the multicomponent drop case, the lightest components resided in the lower stream because they were released early in the drop lifetime. The intermediary components accumulated in the interior of the mixing layer because they were released after the drops were entrained and therefore participated in the mixing process resulting from the double vortex pairing. The heaviest components, which were released later in the drop lifetime, resided in regions of high drop number density. Therefore, a segregation of the chemical species occurs based on the time of their release from the drops. It is this segregation, which is important in combustion and chemical conversion processes, that cannot be captured by the single-component fuel drop approximation.

### Acknowledgment

This research was performed at the Jet Propulsion Laboratory (JPL) of the California Institute of Technology, under the partial sponsorship of the Donors of The Petroleum Research Fund, administered by the American Chemical Society. Additional sponsorship was provided by U.S. Department of Energy (DOE), with Mr. Neil Rossmel (DOE Headquarters) and Mr. D. Hooker (DOE Golden Center) serving as contract monitors, under an agreement with the National Aeronautics and Space Administration. The authors thank Dr. Kenneth Harstad of JPL for many helpful discussions on thermodynamics and Dr. Nora Okong'o of JPL for help with numerical and computational aspects. Computational resources were provided by the supercomputing facility at JPL.

### References

- [1] Boivin, M., Simonin, S. and Squires, K. D., Direct numerical simulation of turbulence modulation by particles in isotropic turbulence, *J. Fluid Mech.*, 375, 235-263, 1998.
- [2] Mashayek, F. and Jaber, F. A., Particle dispersion in forced isotropic low-Mach-number turbulence, *Int. J. Heat Mass Transfer*, 42, 2823-2836, 1999.

- [3] Mashayek, F., Direct numerical simulations of evaporating droplet dispersion in forced low Mach number turbulence, *Int. J. Heat Mass Transfer*, 41(17), 2601-2617, 1998.
- [4] Réveillon, J. and Vervisch, L., Spray vaporization in nonpremixed turbulent combustion modeling: a single drop model, *Comb. Flame*, 121, 75-90, 2000.
- [5] Mashayek, F., Droplet-turbulence interactions in low-Mach-number homogeneous shear two-phase flows, *J. Fluid Mech.*, 367, 163-203, 1998.
- [6] Miller, R. S. and Bellan, J., Direct numerical simulation of a confined three-dimensional gas mixing layer with one evaporating hydrocarbon-droplet laden stream, *J Fluid Mech.*, 384, 293-338, 1999.
- [7] Miller, R. S. and Bellan, J., Direct numerical simulation and subgrid analysis of a transitional droplet laden mixing layer, *Phys. Fluids*, 12(3), 650-671, March 2000.
- [8] Gal-Or, B., Cullinan, Jr., H. T. and Galli, R., New thermodynamic-transport theory for systems with continuous component density distributions, *Chem. Eng. Sci.*, 30, 1085-1092, 1975.
- [9] Cotterman, R. L., Bender, R. and Prausnitz, J. M., Phase equilibria for mixtures containing very many components. Development and application of continuous thermodynamics for chemical process design, *Ind. Eng. Chem. Process Des. Dev.*, 24, 194-203, 1985.
- [10] Tamim, J. and Hallett, W. L. H., A continuous thermodynamics model for multicomponent droplet vaporization, *Chem. Eng. Sci.*, 50(18), 2933-2942, 1995.
- [11] Hallett, W. L. H., A simple model for the vaporization of droplets with large numbers of components, *Combustion and Flame*, 121, 334-344, 2000.
- [12] Lippert, A. M. and Reitz, R. D., Modeling of multicomponent fuels using continuous distributions with application to droplet evaporation and sprays, SAE paper 97FL-468, 1997.
- [13] LeClercq, P. C. and Bellan, J., Direct Numerical Simulation of a temporal mixing layer laden with multicomponent evaporating drops, paper AIAA 2002-0338, presented at the Aerospace Sciences Meeting, Reno, NV, 2002
- [14] Whitson, C. H., Characterizing hydrocarbon plus fractions, *Soc. Pet. Eng. J.*, 23(4), 683-694, 1983.
- [15] Okong'o, N. and Bellan, J., Consistent direct numerical simulation and subgrid scale modeling of a mixing layer laden with evaporating drops, to be submitted for publication, 2002.
- [16] Chou, G. F. and Prausnitz, J. M., Adiabatic flash calculations for continuous or semicontinuous mixtures using an equation of state, *Fluid Phase Equilibria*, 30, 75-82, 1986.
- [17] Williams, F. A., *Combustion Theory*, Addison-Wesley, 1965.
- [18] Miller, R. S., Harstad, K. and Bellan, J., Evaluation of equilibrium and non-equilibrium evaporation models for many-droplet gas-liquid flow simulations, *Int. J. Multiphase Flow*, 24, 1025-1055, 1998.
- [19] Poinso, T. J. and Lele, S. K., Boundary conditions for direct simulations of compressible viscous flows, *J. Comp Phys.*, 101, 104-129, 1992.
- [20] Baum, M., Poinso, T. and Thévenin, D., Accurate boundary conditions for multicomponent reactive flows, *J. Comp. Phys.* 116, 247-261, 1994.
- [21] Moser, R. D. and Rogers, M. M., Mixing transition and the cascade to small scales in a plane mixing layer, *Phys. Fluids A*, 3(5), 1128-1134, 1991.
- [22] Squires, K. D. and Eaton, J. K., Preferential concentration of particles by turbulence, *Phys. Fluids A*, 3(5), 1169-1178, 1991.

Fuel	$\rho_l$	$\theta_{l,0}$	$\sigma_{l,0}$	$\gamma_{l,0}$
n-decane	642	142	-	-
gasoline	742	101	31.5	60.5
diesel	828	185	43.0	60.5

**Table 1:** Parameters characterizing the density and distribution function for different fuels. The density is in  $kg/m^3$  and all parameters related to the distribution function are in  $kg/kmole$ .

Run	$N_d$	$d_0, m$	fuel
SC	$2.28 \times 10^6$	$8.6 \times 10^{-5}$	n-decane
MC	$2.70 \times 10^6$	$7.6 \times 10^{-5}$	diesel

**Table 2:** Simulation parameters. For both simulations  $M_{c,0} = 0.4$ ,  $Re_0 = 500$ ,  $T_{d,0} = 345K$ ,  $T_{g,0} = 375K$  and  $ML = 0.2$ . The initial drop size distribution is polydisperse and Gaussian with  $\langle St_0 \rangle = 3$  and  $St_{0,rms} = 0.5$ .

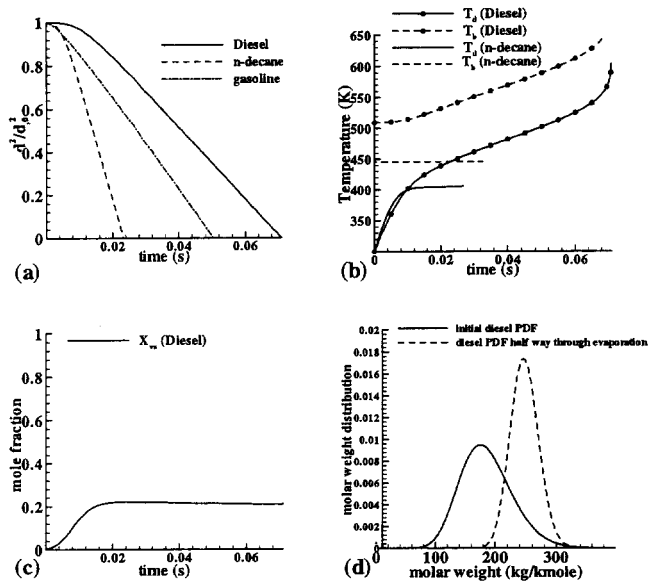


**Figure 1:** Quiescent droplet evaporation. Initial droplet temperature: 300 K. Initial gas temperature: 1000 K. Initial droplet diameter:  $100 \mu m$ . a) Normalized surface area evolution for Diesel, gasoline and n-decane droplets, b) Liquid and boiling temperature evolution, c) Diesel droplet composition evolution (PDF), d) Surface mole fraction during Diesel droplet evaporation.

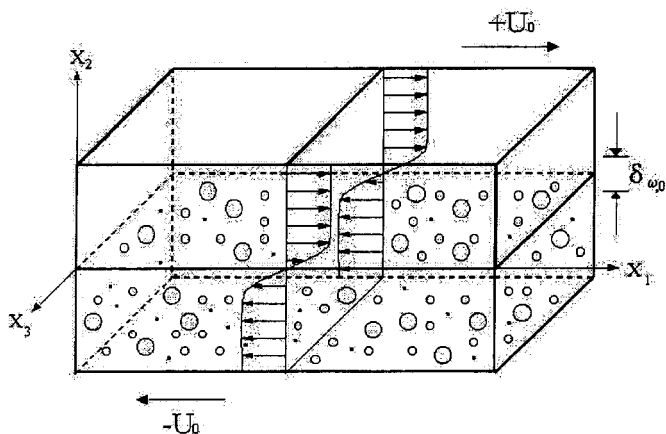


**Figure 2:** Mixing layer configuration.

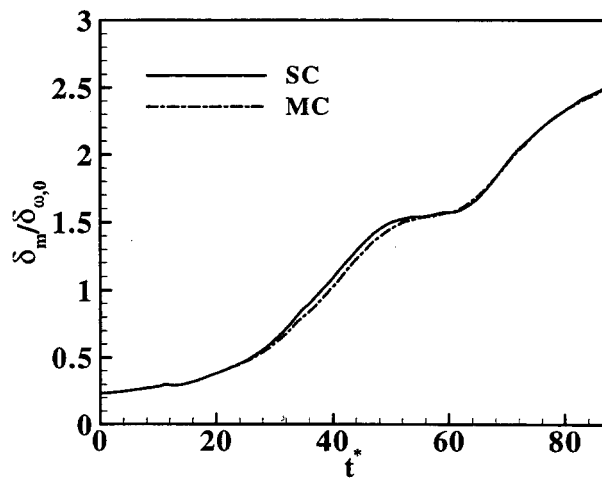


**Figure 3:** Timewise evolution of the momentum thickness for SC and MC simulations.

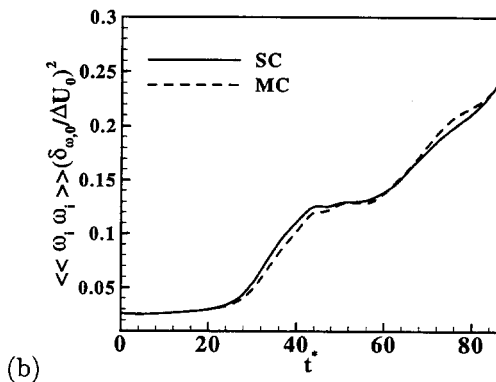
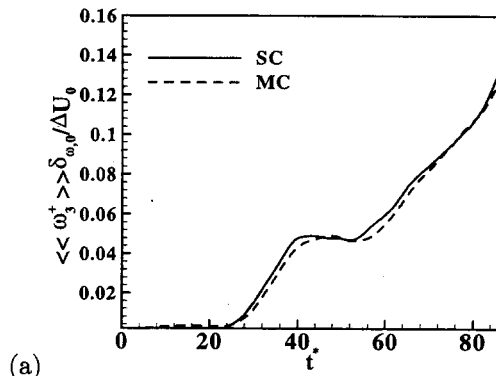


**Figure 4:** a) Volume averaged non-dimensional positive spanwise vorticity. b) Non-dimensional enstrophy.

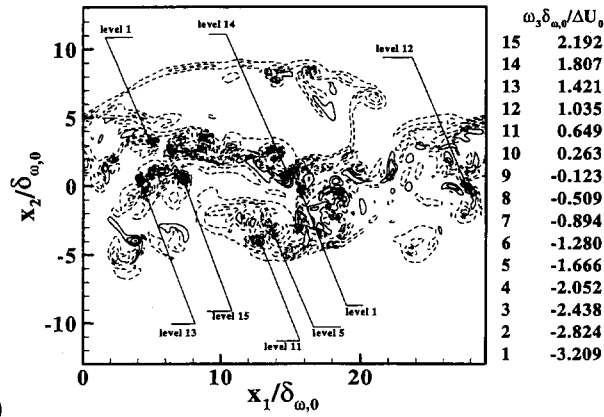
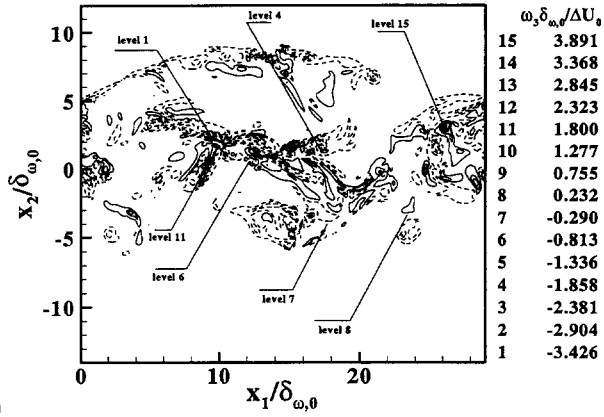


Figure 5: Spanwise vorticity in the between-the-braid plane at  $t^* = 87$ , (a) SC and (b) MC.

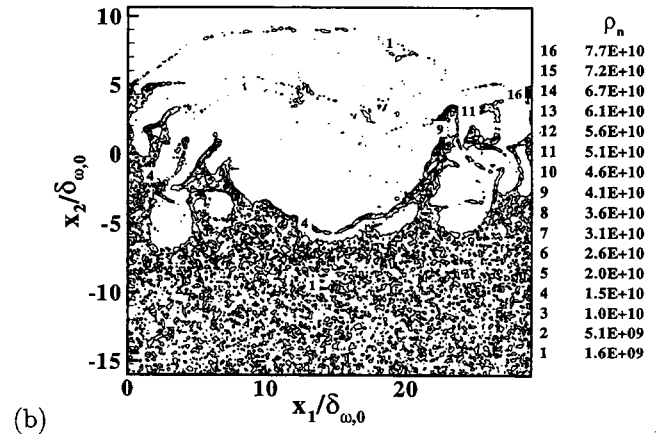
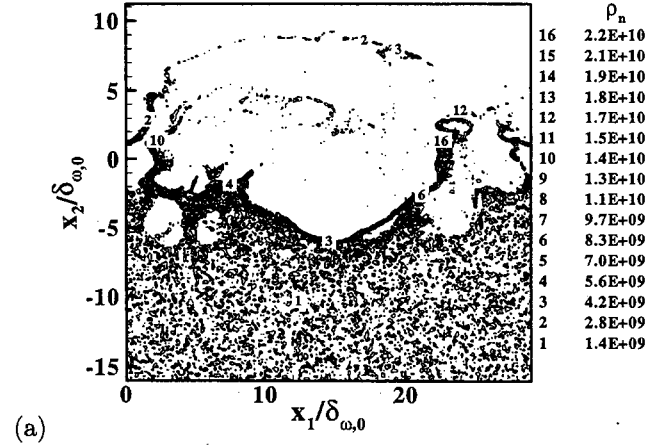


Figure 6: Drop number density in the between-the-braid plane at  $t^* = 87$ , (a) SC and (b) MC.

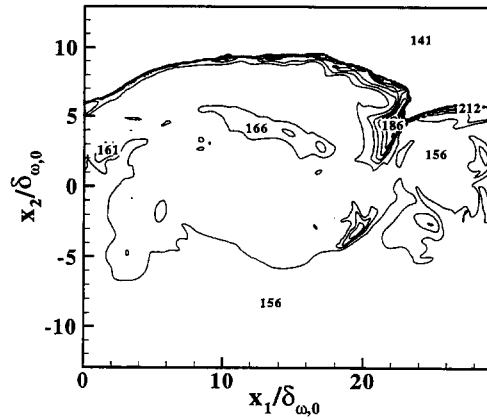


Figure 7: Mean molar weight distribution of the vapor in the between-the-braid plane at  $t^* = 87$ , for the MC simulation.